

# Design and Analysis of Planar Shape Deformation \*

Siu-Wing Cheng<sup>†</sup>, Herbert Edelsbrunner<sup>‡</sup>, Ping Fu<sup>§</sup> and Ka-Po Lam<sup>†</sup>

## Abstract

Shape deformation refers to the continuous change of one geometric object to another. We develop a software tool for planning, analyzing, and visualizing deformations between two shapes in  $\mathbb{R}^2$ . The deformation is generated automatically without any user intervention or specification of feature correspondences. A unique property of the tool is the explicit availability of a two-dimensional shape space, which can be used for designing the deformation either automatically by following constraints and objectives or manually by drawing deformation paths.

## 1 Introduction

This paper describes a method for the deformation of one geometric shape in the plane to another and a software tool that implements it. In computer graphics this operation is commonly referred to as *morphing*. In that area the focus is on the creation of image sequences that display the morph [10, 11, 13]. In contrast, this paper constructs the deformation as a 1-dimensional family of genuine geometric objects.

**Rationale.** This paper follows the general ideas about shape representation and deformation laid out in [3, 4]. It focuses on the special case of two shapes in two dimensions. Even in this simplest of all interesting cases, there is a frightening amount of freedom and an abundant variety of possible deformations. It has been suggested we follow the general trend of making up an evaluation function and compute the optimal deformation defined by that function. The authors of this paper believe that this strategy fails to rationalize the process as it does not eliminate irrational decisions but shift them to a different level. Instead, we follow

\*Research by the first author is partially supported by RGC CERG HKUST 190/95E. Research by the second author is partially supported by NSF under grants CCR-96-19542 and CCR-97-12088.

<sup>†</sup>Department of Computer Science, Hong Kong University of Science and Technology, Kowloon, Hong Kong.

<sup>‡</sup>Department of Computer Science, Duke University, Durham, and Raindrop Geomagic, Research Triangle Park, North Carolina.

<sup>§</sup>Raindrop Geomagic, Research Triangle Park, North Carolina.

a path of deformation design that permits efficient quantitative analysis. The deformations satisfy basic requirements, such as economy in shape variation, local smoothness, and geometric integrity. All constructions are global and mathematically defined and employ natural geometric operations, such as lifting, taking convex hulls, slicing, and projecting. The full description of these constructions and their higher-dimensional interpretations is beyond the scope of this paper and we refer the interested reader to the companion paper [3] published in the same issue of this journal. All claims made in this paper are proved in considerable more generality in [3] and [4], which is the reason this paper adopts a predominantly descriptive rather than analytic style.

The criticism of lacking an optimality criterion and the above response apply only to the automatic reconstruction of deformations. Section 4 explains how the system permits the specification of evaluation functions and the optimization within a two-dimensional space of shapes.

**Summary of results.** The software tool described in this paper constructs and deforms two-dimensional shapes and it rationalizes the process through analysis and visualization. Some of the features of that tool are now listed.

- The source and target shapes are regular sets in  $\mathbb{R}^2$ , that is, each set is the closure of its interior. The sets can have arbitrarily many components and holes. The chosen data structure places no limitations in principle on the kind of shapes although it is better suited for representing some than it is for others.
- The deformation can be computed fully automatically, which means that also the topology of the shape is changed without user intervention. See Figure 1 for an example where a ‘0’ with one hole is deformed into a ‘1’ without hole.
- Each intermediate shape is determined by a time parameter,  $t \in [0, 1]$ , and a size parameter,  $\alpha^2 \in \mathbb{R}$ . In the automatic and unconstrained deformation, the size is a function of  $t$  and the initial and final size values. Deformation paths satisfying shape constraints can be

designed in the two-dimensional shape space of time and size.

- The deformation is monitored by keeping track of quantitative information, such as the area, boundary length, number of components, and number of holes. Constraints guiding the automatic design of a deformation can be formulated in terms of these quantities.

The tool provides VCR functionalities for the interactive visualization, such as play, reverse, step forward, step backward, etc.

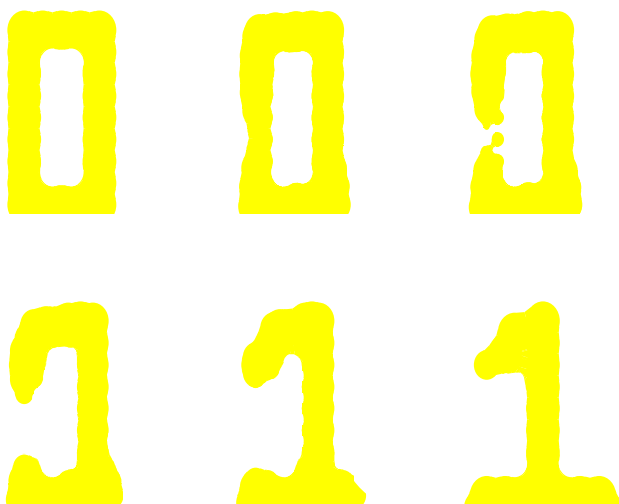


Figure 1: Read the pictures like English text from left to right and rows from top to bottom to see the deformation from ‘0’ to ‘1’.

We should mention that this paper does not address the question how a two-dimensional shape can be turned into the representation used in this paper. That question is difficult and interesting in its own right. The appearance of the shapes for small data sets is similar to the blobby models introduced by Blinn [1] and the union-of-spheres models used by Tam and Fournier [12]. We claimed above that the chosen data structure places no limitations in principle on the kind of shapes that can be represented. Specifically, this means that for any subset of  $\mathbb{R}^2$  and any  $\varepsilon > 0$  we can represent a shape whose Hausdorff distance from that subset is less than  $\varepsilon$ . Beyond Hausdorff distance, our representation can approximate the tangent direction along differentiable boundary segments, but it cannot approximate the curvature along twice differentiable boundary segments. The more important question of how the size of that representation depends on the type of subset and on  $\varepsilon$  is left open.

**Ramifications.** The widespread use of image morphing in the movie and advertisement industries justifies the related

research, maybe also the one reported in this paper. The particular properties and features of the method described in this paper suggests additional applications.

- The shape is well defined at every moment during the deformation. If we stack up all two-dimensional shapes we get a pipe-like three-dimensional shape that smoothly starts, branches, joins, and ends. Such pipes are good models of blood vessels and complicated exhaust systems. The constrained deformation option can be used to maintain, say, a constant cross-section area in the design of such a system.

The construction of pipes is similar to shape reconstruction from slices, which is a widely studied problem in computer graphics [7] and computational geometry [2]. The algorithm developed for this problem are however fundamentally different from the algorithm in this paper because they start from different assumptions on how a cross-section or two-dimensional shape is represented.

- The automatic deformation between two given shapes is canonical. The kind and amount of change can be used to define a distance measure between shapes useful for example in automatic pattern recognition. It might be worth trying out this idea in the classification of printed and possibly even handwritten Chinese characters.
- The shape space embedding the deformations is explicitly given as a two-dimensional strip of pairs  $(t, \alpha^2) \in [0, 1] \times \mathbb{R}$ . If the source and target shapes are significantly different then this space is an index into a rich variety of shapes. This suggests applications in shape compression and the design of shape databases.

This particular application is further developed in [3], where it is used to organize general ideas about shape deformation.

**Outline.** Section 2 reviews the two basic ingredients to our deformation tool: the shape representation of [4] and the deformation technique of [3]. Section 3 explains the various geometric concepts used in the construction and visualized by the software tool. Section 4 discusses the structure of the shape space and how it is exploited in the design of special deformation paths. Section 5 concludes the paper.

## 2 Shape and Deformation

The full details of the shape representation and the shape deformation methods can be found in [4] and in [3]. This section describes only a residual amount of both formalisms and relies on illustrations to provide an intuition for the ideas. Every shape is represented by two data structures: a complex that captures structure and connectivity and a set with differentiable boundary that serves as the appearance of the shape. We explain the two data structures and the deformation method.

**Structure and connectivity.** We begin by specifying the input data, which is a set of weighted points or disks, and the Voronoi decomposition of the plane this set defines. Each disk in the input set  $B = \{b_1, b_2, \dots, b_n\}$  is specified by its center and its radius:  $b_i = (z_i, \varrho_i)$  with  $z_i \in \mathbb{R}^2$  and  $\varrho_i^2 \in \mathbb{R}$ . We permit negative square radii,  $\varrho_i^2$ , which corresponds to imaginary radii,  $\varrho_i$ , and to imaginary disks,  $b_i$ . The *weighted square distance* of a point  $x \in \mathbb{R}^2$  from  $b_i$  is  $\pi_i(x) = \|x - z_i\|^2 - \varrho_i^2$ , and the (*weighted*) *Voronoi cell* of  $b_i$  is the set of points at least as close to  $b_i$  in terms of the weighted square distance function as to any other disk:

$$V_i = \{x \in \mathbb{R}^2 \mid \pi_i(x) \leq \pi_j(x), \text{ for all } j\}.$$

See Figure 2 for an example. The Voronoi cells decompose

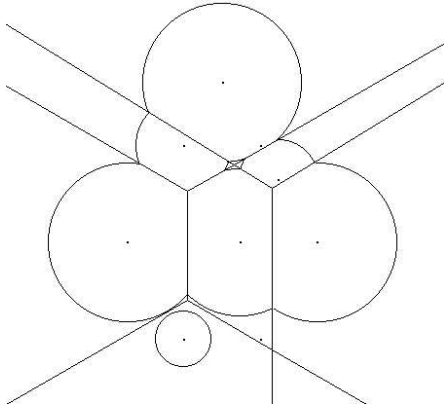


Figure 2: The Voronoi cells of nine disks. Seven of the disks have positive and two have imaginary radii. Two of the centers do not lie in their Voronoi cells.

the union of disks into convex cells:  $\bigcup B = \bigcup_{i=1}^n (V_i \cap b_i)$ . Any two of these cells are either disjoint or they meet along a portion of their boundaries.

The *complex* data structure is denoted as  $\text{Dsx } B$  and records the overlap between the cells  $R_i = V_i \cap b_i$ . Specifically,  $z_i$  is a vertex in  $\text{Dsx } B$  iff  $R_i \neq \emptyset$  and  $z_i z_j$  is an edge iff  $R_i \cap R_j \neq \emptyset$ . Furthermore,  $\text{conv} \{z_i \mid i \in I\}$  is a two-dimensional cell, for  $I$  a set of three or more disk indices, iff  $\bigcap_{i \in I} R_i \neq \emptyset$  and  $I$  is maximal with this property. For  $B$  in general position all cells in  $\text{Dsx } B$  are triangles. However, we cannot reasonably make this simplifying assumption because the deformation method described shortly systematically creates degenerate disk sets, such as the one shown in Figure 2. Even if we have general position at times  $t = 0$  and  $t = 1$ , there are parallelograms in the intermediate complexes, as shown in Figure 3.

**Shape appearance.** The body is defined as a union of an infinite family of disks, and the skin is its boundary, which is the envelope of an infinite family of circles. To define these

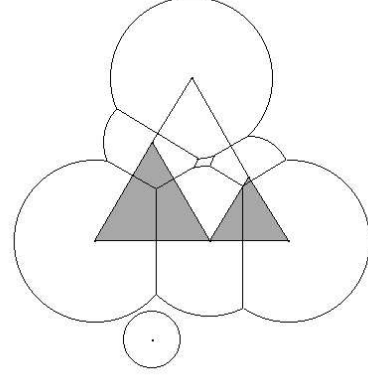


Figure 3: The Voronoi decomposition and complex of the union of disks in Figure 2. The complex contains only two cells, namely the shaded triangles. The transparent parallelogram does not belong to the complex (only its edges do), although it would if the corresponding four disks were large enough to fill the hole.

families, we observe that  $b_i = \pi_i^{-1}(-\infty, 0]$  and its bounding circle is  $\pi_i^{-1}(0)$ . The weighted square distance functions span the usual vector space defined by function addition and scaling. Let  $\Pi = \{\pi_i \mid 1 \leq i \leq n\}$  be the collection of weighted square distance functions defined by  $B$ . The affine hull of  $\Pi$  is the family of combinations  $\sum \gamma_i \cdot \pi_i$ , in which the  $\gamma_i$  add up to 1. The convex hull is the subfamily defined by non-negative scaling factors:

$$\text{conv } \Pi = \left\{ \sum_{i=1}^n \gamma_i \cdot \pi_i \mid \sum_{i=1}^n \gamma_i = 1, \gamma_i \geq 0 \text{ for all } i \right\}.$$

The convex hull is an infinite family of paraboloid functions and we construct the skin and body by shrinking each  $\pi \in \text{conv } \Pi$  using a parameter  $0 \leq s \leq 1$ . For  $\pi(x) = \|x - z\|^2 - \varrho^2$ , we define the shrunken function as

$$\pi^s(x) = \frac{1}{s} \cdot \|x - z\|^2 - \varrho^2.$$

The zero-set of  $\pi^s$  is the circle with center  $z$  and radius  $\sqrt{s}\varrho$ . The envelope and union of the infinite family of shrunken disks is now defined with the help of the pointwise minimum function,  $\Gamma_s(x) = \min\{\pi^s(x) \mid \pi \in \text{conv } \Pi\}$ :

$$\begin{aligned} \text{skin}^s B &= \Gamma_s^{-1}(0), \\ \text{body}^s B &= \Gamma_s^{-1}(-\infty, 0]. \end{aligned}$$

They are referred to as the *s-skin* and the *s-body* of  $B$ , as illustrated in Figure 4.

**Shape deformation.** Fix a parameter  $s \in (0, 1)$  and let  $B$  and  $C$  be two finite sets of disks defining the initial and the final shapes of the deformation. Intermediate shapes are constructed by interpolating between the two sets. It

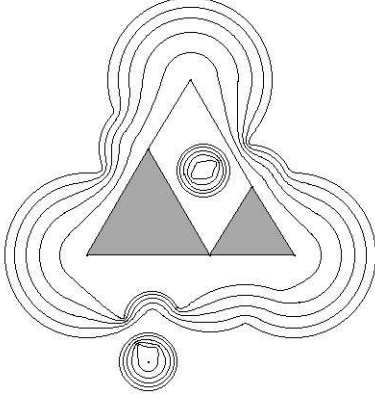


Figure 4: The skins for  $s = 0.1, 0.3, 0.5, 0.7, 0.9$  of the same set of disks as in Figures 2 and 3. Observe that the complex is contained in the five bodies and they are all connected the same way: each has two components of which one has a hole and the other does not.

is convenient to project a cross-section of the vector space of weighted square distance functions onto the set of disks. Formally, if  $b$  and  $c$  are disks with weighted square distance functions  $\pi$  and  $\varphi$  and  $\beta + \gamma = 1$  then  $a = \beta \cdot b + \gamma \cdot c$  is the disk with weighted square distance function  $\beta \cdot \pi + \gamma \cdot \varphi$ . With this introduction, we define

$$\begin{aligned} A_t &= (1-t) \cdot B + t \cdot C \\ &= \{(1-t) \cdot b + t \cdot c \mid b \in B, c \in C\} \end{aligned}$$

for every  $t \in [0, 1]$ . Clearly  $A_0 = B$  and  $A_1 = C$ . For a given value of  $s$ , we thus have a one-parameter family of shapes,  $\mathbb{X}_t = \text{body}^s A_t$ , that deforms the initial shape,  $\mathbb{X}_0 = \text{body}^s B$ , into the final shape,  $\mathbb{X}_1 = \text{body}^s C$ . Figure 5 uses ten snapshots to illustrate the deformation from a shape defined by four disks to one defined by only three disks. Observe the automatic change of topology that happens synchronously for the skin and the complex. In Figure 5, there is a change in topology between all contiguous snapshots except for the last three. Even though the seventh and the eighth snapshots have the same topology, the latter is obtained from the former by two changes, one filling a hole and one opening a hole. The second, third, fourth, and sixth snapshots are taken right at the time of topology changes when two components or two portions of the same component touch in a point and locally separate the complement.

### 3 Visualization of Concepts

The display panel of the software tool can be used to visualize all geometric concepts mentioned in Section 2 and more. As mentioned earlier, the expositions of these concepts are primarily descriptive.

**Basic structures.** Let  $B$  be a finite set of disks as before. The (weighted) Voronoi complex, denoted as  $\text{Vor } B$ , is the collection of two-dimensional Voronoi cells together with common intersections among them. The (weighted) Delaunay complex, denoted as  $\text{Del } B$ , records the overlap among two-dimensional Voronoi cells, as shown in Figure 6 to the right.

Next we discuss a nested sequence of subcomplexes of the Delaunay complex. Let  $\alpha^2 \in \mathbb{R}$  and define  $b_i(\alpha)$  as the disk with center  $z_i$  and radius  $\sqrt{\varrho_i^2 + \alpha^2}$ . We have  $b_i(0) = b_i$ , and if  $\varrho_i^2 = 0$  then the radius of  $b_i(\alpha)$  is  $\alpha$ . Let  $B(\alpha) = \{b_i(\alpha) \mid b_i \in B\}$  and observe that the Voronoi complex of  $B(\alpha)$  is the same as that of  $B$ . In other words, the Voronoi complex and the Delaunay complex do not vary with  $\alpha^2$ . The cells of the convex decomposition of  $\bigcup B(\alpha)$  grow with  $\alpha$ :

$$R_i(\alpha_1) = V_i \cap b_i(\alpha_1) \subseteq V_i \cap b_i(\alpha_2) = R_i(\alpha_2)$$

whenever  $\alpha_1 \leq \alpha_2$ . We call  $\text{Dsx}_\alpha B = \text{Dsx } B(\alpha)$  the  $\alpha$ -complex of  $B$ . The collection of such complexes is nested and the last one is the Delaunay complex:

$$\emptyset = \text{Dsx}_{\alpha_0} B \subseteq \text{Dsx}_{\alpha_1} B \subseteq \text{Dsx}_{\alpha_2} B = \text{Del } B,$$

where  $\alpha_0^2$  is sufficiently small,  $\alpha_2^2$  is sufficiently large, and  $\alpha_0^2 \leq \alpha_1^2 \leq \alpha_2^2$ . Figure 6 illustrates the sequence of  $\alpha$ -complexes by showing four of a much larger number of nested complexes defined by the nine disks used in Figures 2, 3, and 4.

**Decomposed skin and body.** Similar to the union of disk, we can decompose the skin and the body into simple pieces. The complex that produces the decomposition consists of two-dimensional Voronoi cells, two-dimensional Delaunay cells, and rectangles that are Cartesian products of matching Voronoi and Delaunay edges. All these cells are shrunk so they fit together to form a decomposition of  $\mathbb{R}^2$ . To describe this complex, let  $s \in [0, 1]$  be arbitrary but fixed. Let  $I$  be a subset of indices with

$$\begin{aligned} \nu_I &= \bigcap_{i \in I} V_i \in \text{Vor } B, \\ \delta_I &= \text{conv} \{z_i \mid i \in I\} \in \text{Del } B. \end{aligned}$$

The dimension of  $\nu_I$  is  $k \in \{0, 1, 2\}$  and that of  $\delta_I$  is  $2 - k$ . The corresponding (two-dimensional) cell in the complex is

$$\mu_I^s = s \cdot \nu_I + (1-s) \cdot \delta_I,$$

where addition and scaling refer to the operations in the vector space of points in  $\mathbb{R}^2$ . The  $s$ -mixed complex, denoted as  $\text{Mix}^s B$ , consist of all cells  $\mu_I^s$  and all non-empty common intersections among them. Figure 7 illustrates the mixed complex along with the skin and the complex for the nine disks used in earlier figures.

Observe that  $\text{Mix}^0 B = \text{Del } B$  and  $\text{Mix}^1 B = \text{Vor } B$ . For all other values of  $s$ ,  $\text{Mix}^s B$  contains a shrunken copy of

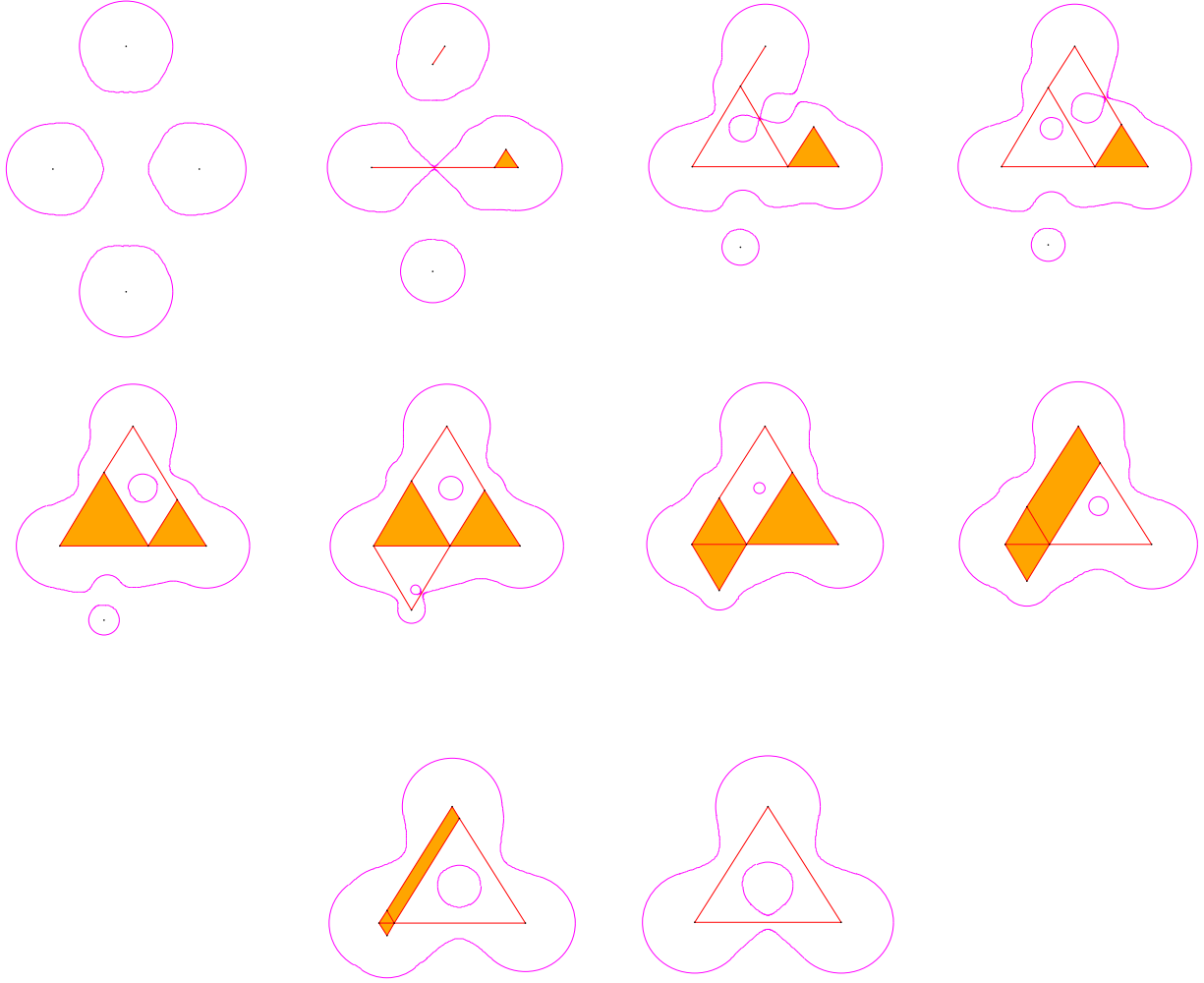


Figure 5: Ten snapshots of a deformation with complex and skin displayed. The parameter  $s$  for all shapes is 0.5. The set of disks that generates the complex and the skin in the fifth snapshot is the same as in Figures 2, 3, and 4.

every Voronoi cell and every Delaunay cell. The shrunken copy of  $V_i$  intersects  $\text{skin}^s B$  in a collection of arcs that all belong to a common circle, namely the zero-set of  $\pi_i^s$ . Similarly, the shrunken copy of a Delaunay cell intersects the skin in a collection of arcs that all belong to a common circle. We note that the body lies outside that circle. The remaining two-dimensional cells in  $\text{Mix}^s B$  are rectangles, and each rectangle intersects the skin in a collection of arcs that belong to a common hyperbola. A more detailed description of the skin decomposition including formulas for all circles and hyperbolas can be found in [4].

**Complementarity.** We develop an explicit expression of the symmetry between shape and complement by introducing another set of disks. Call two disks  $b_i = (z_i, \varrho_i)$  and  $b_j^\perp = (y_j, \rho_j)$  *orthogonal* if

$$\|z_i - y_j\|^2 = \varrho_i^2 + \rho_j^2,$$

and *further than orthogonal* if the square distance between the centers exceeds the sum of square radii. In case of real radii the bounding circles of two orthogonal disks meet at right angles. We construct a new set of disks,  $B^\perp = \{b_1^\perp, b_2^\perp, \dots, b_m^\perp\}$ , that cover the part of  $\mathbb{R}^2$  outside  $\bigcup B$  and overlap the disks in  $B$  orthogonally or less. Specifically, for each vertex  $y_j$  of  $\text{Vor } B$  choose the radius  $\rho_j$  such that  $b_j^\perp = (y_j, \rho_j)$  is orthogonal to all  $b_i$  with  $y_j \in V_i$ . By definition of Voronoi complex,  $b_j^\perp$  is further than orthogonal from all other disks in  $B$ . For completeness, we stipulate a Voronoi vertex at infinity in the direction of each unbounded Voronoi edge and define the corresponding disk as a half-plane. It is not difficult to see that  $\text{Vor } B = \text{Del } B^\perp$  and  $\text{Del } B = \text{Vor } B^\perp$ , and therefore  $(B^\perp)^\perp = B$ . An additional noteworthy property is the complementarity of the two bod-

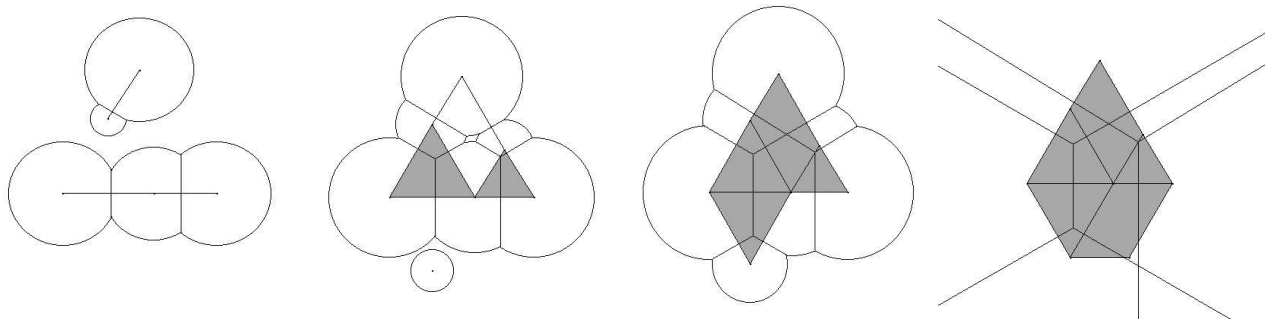


Figure 6: Decomposed disk union and  $\alpha$ -complex for four values of  $\alpha$ . In the second example, we have  $\alpha = 0$  and therefore the same complex as in Figure 3. In the fourth example, we have  $\alpha$  sufficiently large so that the  $\alpha$ -complex is the Delaunay complex.

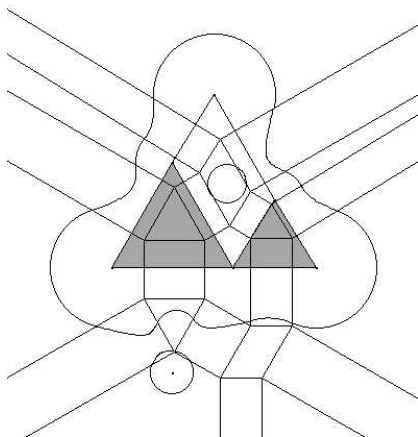


Figure 7: The 0.5-skin of the disk set in Figure 2 is decomposed into circle and hyperbola arcs by the 0.5-mixed complex.

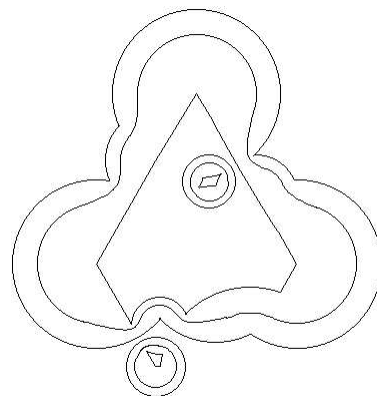


Figure 8: The boundary of  $\bigcup B$ , the boundary of  $\bigcup B^\perp$ , and the common 0.5-skin of  $B$  and  $B^\perp$  separating the two boundaries.

ies. Formally,

$$\begin{aligned} \text{body}^s B \cup \text{body}^{1-s} B^\perp &= \mathbb{R}^2, \\ \text{body}^s B \cap \text{body}^{1-s} B^\perp &= \text{skin}^s B \\ &= \text{skin}^{1-s} B^\perp. \end{aligned}$$

Figure 8 illustrates the relationship between  $B$  and  $B^\perp$  by showing three skins of  $B$ , for  $s = 0.0, 0.5, 1.0$ . The 0-body of  $B$  is the closed complement of a union of disks, namely of  $\bigcup B^\perp$ . The 0.5-skin shrinks away from the boundaries of  $\bigcup B$  and of  $\bigcup B^\perp$  and lies between  $\text{skin}^0 B = \text{skin}^1 B^\perp$  and  $\text{skin}^1 B = \text{skin}^0 B^\perp$ .

**Deformation and topology change.** We return to the deformation constructed by interpolating disk sets:  $A_t = (1 - t) \cdot B + t \cdot C$ , as explained in Section 2. Letting  $s \in (0, 1)$  be fixed and  $t$  vary inside  $[0, 1]$ , we generate a 1-parameter family of shapes,  $\mathbb{X}_t = \text{body}^s A_t$ . We focus on the local picture of a change in topology as  $t$  varies continuously. Each change occurs at a particular moment in time and a particular point in the plane. Let this point be  $z$  and distinguish three

cases depending on the type of cell in the mixed complex that contains  $z$ .

**CASE  $I = \{i\}$ .** The point  $z$  lies inside the shrunken Voronoi cell  $\mu_I^s$ . The cell specifies the portion of the circle defined by  $b_i$  that belongs to the skin. This circle is the zero-set of  $\pi_i^s$ . In the non-degenerate case, the radius of this circle is either imaginary or positive real. The topology change happens at the transition from the former to the latter case, or vice versa. This transition either creates a new component by growing a disk from  $z$  or it removes a component by shrinking a disk to  $z$ .

**CASE  $I = \{i, j\}$ .** The point  $z$  lies inside the rectangle  $\mu_I^s$ . The rectangle specifies the portion of the hyperbola defined by  $b_i$  and  $b_j$  that belongs to the skin. The hyperbola consists of two branches living in diagonally opposite quadrants defined by the two asymptotic lines, as illustrated in Figure 9. In the non-degenerate case, the two branches either locally separate or locally sandwich the body. The topology change happens at the transition when the hyperbola equals the two asymptotic lines and flips from one pair of opposite quadrants to the other.

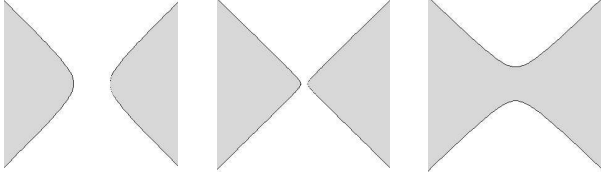


Figure 9: From left to right the sequence illustrates the creation of a bridge through flipping a hyperbola. From right to left it illustrates the removal of that bridge.

The transition either creates a bridge by locally joining two portions of the body at  $z$ , or it removes a bridge by locally separating two portions at  $z$ .

CASE  $I = \{i, j, k\}$ . The point  $z$  lies inside the shrunken Delaunay triangle  $\mu_I^s$ . In degenerate configurations  $I$  may contain more than three indices and  $\mu_I^s$  may have more than three sides. The triangle specifies the portion of the circle defined by  $b_i^\perp$  orthogonal to  $b_i, b_j, b_k$  that belongs to the skin. Observe the symmetry to card  $I = 1$ . In the non-degenerate case, the radius of the circle is either positive real or imaginary. The transition either removes a hole by shrinking a disk to  $z$  or it creates a hole by growing a disk from  $z$ .

Note that the points  $z$  where a topological change happens are centers of disks (in  $B$  or in  $B^\perp$ ) or apices of hyperbolas. It is also possible that the center of a circle or the apex of a hyperbola does not lie inside the corresponding mixed cell. In this case, that point is not the location of a topological change.

**Asymmetry of deformation.** For a fixed  $t \in [0, 1]$ ,  $A_t = (1-t) \cdot B + t \cdot C$  is a set of disk and we consider its Voronoi and Delaunay complexes, as shown in Figure 10. Combinatorially, the Delaunay complex changes only twice, from  $t = 0$  to  $t \in (0, 1)$  to  $t = 1$ . Geometrically, it moves all the time as the cells gradually change shape. Interestingly, the situation is different for the Voronoi complex, and this in spite of the symmetry between the two complexes noted above. The Voronoi complexes of the  $A_t$  are the same for all  $t \in (0, 1)$ . Specifically, each such Voronoi complex is the overlay of  $\text{Vor } A_0$  and  $\text{Vor } A_1$ , as can be seen in Figure 10. The asymmetry is explained by the asymmetry of the deformation. An alternative definition of deformation uses the shapes defined by the complementary disk sets:

$$D_t^\perp = (1-t) \cdot B^\perp + t \cdot C^\perp.$$

$D_t^\perp$  is different from  $A_t^\perp$  except at the beginning, at  $t = 0$ , and at the end, at  $t = 1$ . To see that the two are indeed different, in general, note that  $(A_t^\perp)^\perp = A_t$ . So when  $A_t^\perp$  changes as  $t$  increases, the Voronoi complex changes and the Delaunay complex is invariant. On the other hand, when  $D_t^\perp$  changes as  $t$  increases, the Delaunay complex changes and the Voronoi complex is invariant.

## 4 Deformation Design

The control panel of the software tool contains the VCR buttons that drive the deformation through the selection and alteration of time and size. The explicit representation of the two-dimensional shape space permits the rational design of deformations.

**Shape space.** Fix a value of  $s \in (0, 1)$  and let  $B$  and  $C$  be the two disk sets that define the initial and the final shape of a deformation problem. We have an intermediate shape defined for each value  $t \in [0, 1]$  of the time parameter and each value  $\alpha^2 \in \mathbb{R}$  of the size parameter. Specifically, each such intermediate shape is defined by the set of disks  $A_t(\alpha)$ , where  $A_t = (1-t) \cdot B + t \cdot C$ . We use  $(t, \alpha^2)$  as a coordinate pair to specify shapes in

$$\Omega = [0, 1] \times \mathbb{R},$$

which we refer to as *shape* or *state space*.  $\Omega$  is a two-dimensional strip that can be decomposed into regions within which the shape variation is insignificant. As an example consider the decomposition into shapes whose complexes are the same:  $\mathbb{X}_1 = \text{body } A_{t_1}(\alpha_1)$  and  $\mathbb{X}_2 = \text{body } A_{t_2}(\alpha_2)$  are *similar* if  $\text{Dsx}_{\alpha_1} A_{t_1} = \text{Dsx}_{\alpha_2} A_{t_2}$ .

Since the moments in time the two shapes exist are in general different this needs some clarification. Although the Delaunay complex moves with time, its combinatorial structure is the same during the entire open time interval. We therefore have an unambiguous notion of sameness for Delaunay cells over time and it makes sense to refer to a Delaunay cell  $\delta_I$  without specifying the time, which can be anywhere in  $(0, 1)$ . Two complexes at different moments in time are the *same* if they contain the same cells. Similarity among shapes is therefore well defined and it is an equivalent relation.

**Curve arrangement.** We gain insight into the decomposition of  $\Omega$  by considering a single Delaunay cell,  $\delta_I$ . For each time  $t \in (0, 1)$ , we define  $f_I(t)$  such that  $\delta_I(t)$  belongs to  $\text{Dsx}_\alpha A_t$  iff  $\alpha^2 \geq f_I(t)$ . For each two-dimensional  $\delta_I$  the discriminating function is linear:

$$f_I(t) = a_1 \cdot t + a_0.$$

For Delaunay edges and vertices the description of  $f_I$  is made complicated by the somewhat technical distinction between attached and unattached cells, which is explained in some detail in [6]. A cell  $\delta_I$  is *attached* at time  $t$  if for every  $\alpha^2 \in \mathbb{R}$  the presence of  $\delta_I(t)$  in  $\text{Dsx}_\alpha A_t$  implies the presence of a higher-dimensional cell,  $\delta_J$ , that contains  $\delta_I$  as a face. Since  $\delta_J$  cannot be in the complex without its faces this implies  $f_I(t) = f_J(t)$  for this value of  $t$ . The interesting case is when  $\delta_I(t)$  is unattached. For example if  $\delta_I$  is two-dimensional then it is unattached during the entire open time interval. In general,  $\delta_I$  is unattached during a single

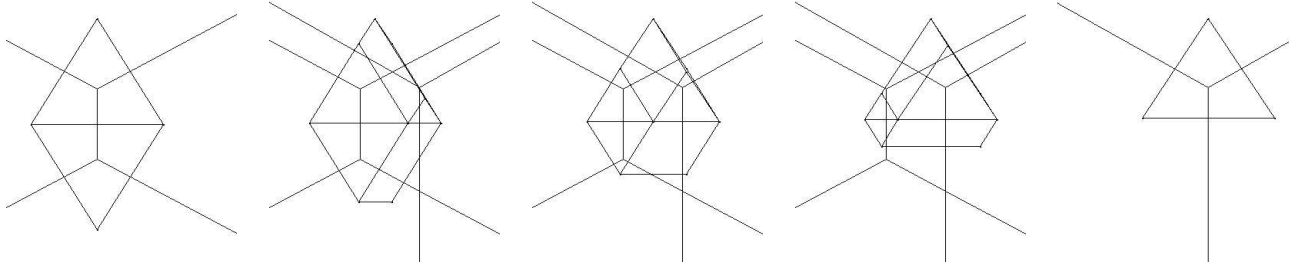


Figure 10: The Voronoi and Delaunay complexes at times  $t = 0.0, 0.25, 0.5, 0.75, 1.0$  during the deformation.

and possibly empty time interval. In that time interval, the discriminating function is at most quadratic:

$$f_I(t) = a_2 \cdot t^2 + a_1 \cdot t + a_0,$$

with  $a_2 \leq 0$ . We picture  $\Omega$  and its decomposition by drawing time from left to right and size from bottom to top. The graphs of the discriminating functions are lines that pass through the strip from left to right and upside-down parabolas that begin and end on the strip boundary or on graphs of other discriminating functions, as shown in Figure 11. The

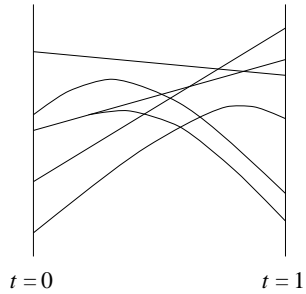


Figure 11: The decomposition of  $\Omega$  into regions of similar shapes. All curves are pieces of lines and parabolas.

graphs decompose  $\Omega$  into regions of similar shapes. It can however happen that two similar shapes correspond to points in different regions. In this case there is no deformation representable in  $\Omega$  that transforms one shape to the other and uses only similar shapes.

**Designing in shape space.** The initial shape corresponds to the point  $P_0 = (0, 0)$  in  $\Omega$  and the final shape corresponds to  $P_1 = (1, 0)$ . Every continuous deformation between the two shapes that can be represented in our framework corresponds to a path  $p : [0, 1] \rightarrow \Omega$  with  $p(0) = P_0$  and  $p(1) = P_1$ . For example the basic deformation described in Section 2 corresponds to the straight line segment connecting  $P_0$  with  $P_1$ , which is the image of the path  $p(u) = (u, 0)$ . It may be that more complicated paths give better deformations and we describe how the decomposition of  $\Omega$  can be used to find such paths.

An important first step in the rational design of deformations is the computation of *signatures* that are functions from  $\Omega$  to  $\mathbb{R}$ . An example is the area signature that maps each  $(t, \alpha^2)$  to the area of the corresponding body. Strictly speaking that area also depends on the value of the parameter  $s$  and we have a signature for each  $0 \leq s \leq 1$ . Another example is the connectivity of shapes captured by two signatures,  $\beta_0, \beta_1 : \Omega \rightarrow \mathbb{R}$ , counting components and holes.  $\beta_0$  and  $\beta_1$  are independent of  $s$  and can be computed directly from the complex, which is homotopy equivalent to the body of the shape [4].

Let  $\mathcal{G}$  be the dual graph of the decomposition of  $\Omega$  created by the arrangement of lines and parabolas described above. Let  $\beta_0(\nu)$  be the number of components and  $\beta_1(\nu)$  be the number of holes of any one shape represented by the region or node  $\nu$  in  $\mathcal{G}$ . Let  $\mu_0$  and  $\mu_1$  be the nodes whose regions contain  $P_0$  and  $P_1$  in their boundaries. A non-degenerate path,  $p : [0, 1] \rightarrow \Omega$ , traces out a sequence of regions and thus translates into a discrete path in  $\mathcal{G}$ :  $\mu_0 = \nu_0, \nu_1, \dots, \nu_\ell = \mu_1$ . Suppose we are interested in a deformation that goes through as few topological changes as possible. The number of such changes that occur along the path  $p$  is a sum of absolute differences:

$$\sum_{i=1}^{\ell} |\beta_0(\nu_i) - \beta_0(\nu_{i-1})| + |\beta_1(\nu_i) - \beta_1(\nu_{i-1})|.$$

Think of the term inside the sum as the length of the arc connecting nodes  $\nu_{i-1}$  and  $\nu_i$ . The problem of finding a path in  $\Omega$  with minimum number of topological changes thus reduces to finding a shortest path in  $\mathcal{G}$ , which can be solved by standard graph algorithms. An improvement of this approach based on the monotonicity of minimizing paths is described in [9].

## 5 Discussion

This paper describes a method for the automatic deformation of shapes in  $\mathbb{R}^2$  and a software tool that implements it. The exposition is primarily descriptive and proofs (of more general claims) can be found in the companion paper [3] and in [4].

**Algorithms.** The primary algorithmic problem that arises as part of the deformation method is the construction of the 1-parameter family of Delaunay complexes  $\text{Del } A_t$ , for  $t \in [0, 1]$ . As explained in [3], this problem reduces to computing a 4-dimensional convex hull, or equivalently a three-dimensional (weighted) Delaunay complex. In the latter interpretation, the third coordinate is time and  $\text{Del } A_t$  is the cross-section at  $x_3 = t$ .  $\text{Dsx } A_t$  is a subcomplex of  $\text{Del } A_t$  and the body and skin of the shape are computed from that subcomplex. Our software tool uses the three-dimensional Delaunay complex algorithm mentioned in [6] and selects subcomplexes as explained in the same reference.

A second interesting algorithmic problem is the construction of the line and parabola arrangement that decomposes the shape space. We implemented the incremental algorithm of [5]. The decomposition is typically too fine to be of much use within the user interface. A coarsened version of that decomposition, obtained for example by snap-rounding as described in [8], might be more useful than the actual arrangement.

**Extensions.** There are means to impose structure on the shape space other than the arrangement of lines and parabolas described in Section 4. Take for example the area signature,  $a : \Omega \rightarrow \mathbb{R}$ , say for  $s = 0.5$ . It is continuous and increases with growing  $\alpha^2$ . Each level set,  $a^{-1}(c)$ , is therefore a monotone path connecting a point on the left with a point on the right boundary of  $\Omega$ . If  $P_0$  and  $P_1$  are these two points then  $a^{-1}(c)$  describes an area preserving deformation between the two corresponding shapes.

Applications in data compression and databases for shapes will find the restriction to two base shapes unreasonably limiting. As explained in [3], the mathematical framework for deformation readily extends to any fixed number of base shapes. However, all algorithmic problems get significantly harder as the dimension of the shape space increases.

## References

- [1] J. BLINN. A generalization of algebraic surface drawing. *ACM Trans. Graphics* **2** (1980), 235–256.
- [2] J.-D. BOISSONNAT. Shape reconstruction from planar cross sections. *Comput. Vision, Graphics, Image Process.* **44** (1988), 1–29.
- [3] H.-L. CHENG, H. EDELSBRUNNER AND P. FU. Shape space from deformation. This journal, 2001.
- [4] H. EDELSBRUNNER. Deformable smooth surface design. *Discrete Comput. Geom.*, **21** (1999), 87–115.
- [5] H. EDELSBRUNNER, L. J. GUIBAS, J. PACH, R. POLLACK, R. SEIDEL AND M. SHARIR. Arrangements of curves in the plane-topology, combinatorics and algorithms. *Theoret. Comput. Sci.* **92** (1992), 319–336.
- [6] H. EDELSBRUNNER AND E. P. MÜCKE. Three-dimensional alpha shapes. *ACM Trans. Graphics* **13** (1994), 43–72.
- [7] H. FUCHS, Z. M. KEDEM AND S. P. USELTON. Optimal surface reconstruction from planar contours. *Commun. ACM* **20** (1977), 693–702.
- [8] L. J. GUIBAS AND D. MARIMONT. Rounding arrangements dynamically. In “Proc. 11th Ann. Sympos. Comput. Geom. 1995”, 190–199.
- [9] K. P. LAM. Two-dimensional geometric morphing. Master thesis, Dept. Comput. Sci., Hong Kong University of Science and Technology, 1996.
- [10] S. Y. LEE, K. Y. CHWA, J. HAHN AND S. Y. SHIN. Image morphing using deformation techniques. *J. Visualization Comput. Animation* **7** (1996), 3–23.
- [11] S. M. SEITZ AND C. R. DYER. View morphing. *Computer Graphics* **50** (1996), 21–30.
- [12] R. C. TAM AND A. FOURNIER. Image interpolation using unions of spheres. *The Visual Computer* **14** (1998), 401–413.
- [13] G. WOLBERG. Recent advances in image morphing. In “Proc. Computer Graphics Internat. 1996”, 64–71.